Science and Technology for Energy Transition **77**, 12 (2022)

https://doi.org/10.2516/stet/2022012

Available online at:
stet-review.org

REGULAR ARTICLE OPEN ACCESS

Numerical investigation on flow and heat transfer characteristics of supercritical methane–ethane mixture in a straight channel

Yue Wang[1,2,a], Yue Li[1,2,a], Jie Chen[3], Qian Li[1,2,*], and Weihua Cai[1,2,*]

[1] Laboratory of Thermo-Fluid Science and Nuclear Engineering, Northeast Electric Power University, 132012 Jilin, China
[2] School of Energy and Power Engineering, Northeast Electric Power University, 132012 Jilin, China
[3] CNOOC Gas and Power Group, 100027 Beijing, China

Received: 19 October 2021 / Accepted: 21 April 2022

Abstract. Printed Circuit Heat Exchanger (PCHE) is considered as a promising heat exchanger for offshore Liquefied Natural Gas (LNG) production due to its compactness and high efficiency. To reveal the flow and heat transfer performance of real component nature gas mixture in PCHE, numerical study was conducted to obtain flow and heat transfer characteristics of supercritical methane–ethane mixture in a straight channel of PCHE. The influence of operating parameters including inlet temperature, mass flux and outlet pressure are investigated. The simulation results show that heat transfer coefficient and pressure drop increase with the increase of inlet temperature and mass flux, and decrease with the increase of outlet pressure. The overall variation tendency of heat transfer coefficient and pressure drop in supercritical methane–ethane mixture flow was similar to those in supercritical methane flow, but there still exists some difference due to their different physical properties. For the value of heat transfer coefficient, supercritical methane flow is about 7% larger than that of supercritical methane–ethane mixture flow. And for frictional pressure drop, supercritical methane flow is much larger by about 12%. Finally, new correlations were proposed for supercritical methane–ethane mixture flow, which are helpful for a more accurate flow and heat transfer calculation in PCHE designing for natural gas.

Keywords: Liquefied natural gas, Supercritical methane–ethane mixture, Printed circuit heat exchanger, Thermal performance, Numerical simulation.

Nomenclature

A	Cross-section area of inlet, m^2
C_p	Specific heat at constant pressure, J kg^{-1} K
D_h	Hydraulic diameter, m
f	Fanning friction factor
h	Heat transfer coefficient, W m^{-2} K
L	Length of the channel, m
Nu	Nusselt number
P	Pressure, MPa
ΔP	Pressure drop, MPa
Pr	Prandtl number
q	Heat flux (W m^{-2})
Re	Reynolds number
T	Temperature, K
u	Velocity vector, m s^{-1}
	Greek symbols
λ	Thermal conductivity, W m^{-1} K^{-1}
μ	Dynamic viscosity, Pa s
ρ	Density, kg m^{-3}
	Subscripts
b	Average
in	Inlet
out	Outlet
w	Wall
cr	Critical value

* Corresponding authors: liqian@neepu.edu.cn; caiwh@neepu.edu.cn
[a] Contributed equally to this work.

1 Introduction

Recently, Liquefied Natural Gas (LNG) technology has caught much interest worldwide. In the general trend of industry development and energy structure change, the consumption of Natural Gas (NG) has a rapid increase [1]. The underdeveloped storage and transportation technology of NG, especially for offshore NG, is urgent to be improved to meet this huge demand of NG [2–4]. In order to expand the exploiting of offshore NG, Liquified Natural Gas-Floating Production Storage and Offloading (LNG-FPSO) had been proposed, where space and weight saving are imperative [5]. In LNG-FPSO, heat exchanger, working as a cooler between natural gas compressors, is a key component ensuring the safety, efficiency and compactness. However, the traditional heat transfer exchangers, such as shell-and-tube heat exchanger, are hard to satisfy the high level of compaction. Printed Circuit Heat Exchanger (PCHE), as a new kind of highly compact and efficient channel heat exchanger, is expected to play an important role in meeting the requirement of LNG-FPSO [6–8].

PCHE was primordially put forward in 1985 by *British Company of Heatric* and now has been commercially used [9]. Typically, a PCHE consists of stacked plates, diffusion bonded, with each plate bestrews chemically-etched channels [10]. Four kinds of channels are mainly considered for PCHE, namely straight, zigzag, sinusoidal and airfoil shape, with various of working fluids, such as supercritical CO_2, supercritical nitrogen and supercritical helium. The numerical study of Chai and Tassou [11] on supercritical CO_2 flowed in a PCHE straight channel indicated that heat transfer and pressure drop were enlarged simultaneously at higher mass flux. The same growth rule was also shown in the work of Jeon *et al.* [12] in cross flow condition. While in the study of Marchionni *et al.* [13], the results showed that mass flow rate should not be too large since it would have a negative effect on the efficiency of heat exchanger. Comparing to straight channel PCHE, Meshram *et al.* [14] found that heat transfer had a better performance in zigzag channel, where larger bend angle and smaller linear pitch were preferred within a certain range. While in excessive value, the study of Lee and Kim [15] indicated that heat flux decreased with larger bend angle. Zheng *et al.* [16] visualized vortex structures in a zigzag channel and found that fluid velocity fluctuated remarkably, which benefited the promotion of heat transfer efficiency. Basing on a zigzag channel with smooth fillet, Yang *et al.* [17] pointed out that narrowing cross section of channel could increase the heat transfer rate. By experimentally investigating flow and heat transfer characteristics of supercritical CO_2 (S–CO_2) in PCHE, Nikitin *et al.* [18] developed correlations for Nusselt number (Nu) and Fanning fraction factor (f). Further on, Ishizuka *et al.* [19] developed correlations with wider application scope of Reynolds number (Re) and Baik *et al.* [20] similarly developed correlations for Nu and f based on the same model. Since S–CO_2 typically works near the critical point in S–CO_2 power conversion systems, Bae *et al.* [21] compared existing correlations with experimental data of two-phase CO_2 flow. The comparison indicated that the correlations proposed by Baik *et al.* [20] had the best agreement with experimental results. Hu *et al.* conducted experiments with two-phase R22 as flow media and obtained both heat transfer and flow correlations [22, 23]. For friction factors, Kim *et al.* [24] realized that no correlations had proposed for single-phase flow to include the influence of different temperature and angular dependencies for a wide Reynolds number range. Based on the comparison of results from Computational Fluid Dynamics (CFD) with experimentally obtained correlations, they came up with a new CFD-aided correlation covering an extended range of Reynolds number 2000–58 000 for Nu and f. In the numerical study of flow and heat transfer characteristics for supercritical nitrogen in a cold PCHE channel by Zhao *et al.* [25], correlations for Nu and f were also proposed and validated by experimental data. Kim *et al.* [26] researched thermal-hydraulic performances of PCHE by the KAIST helium test loop and numerical simulations. It indicated that the local pitch-averaged Nusselt number correlations from numerical simulations were more appropriate than the global Nusselt number correlations developed from experimental data.

However, studies on flow and heat transfer performance of supercritical LNG in PCHE channels under low temperature and high-pressure conditions are booming much later in this decade. Zhao *et al.* [27] numerically investigated the effects of airfoil fin arrangement on heat transfer and flow resistance using supercritical LNG as working fluid. The results showed that airfoil-fin PCHE had the better thermal-hydraulic performance than that of straight PCHE. Besides, airfoil fins with staggered arrangement displayed better thermal performance than that with parallel arrangement. Then, further investigations focused on thermal-hydraulic performances of supercritical LNG in zigzag channels of PCHE [28]. The ratio of Nusselt number to Euler number was proposed to evaluate comprehensive heat transfer performance of PCHE. By analyzing heat transfer and pressure drop characteristics, the better bend angle and operating conditions were confirmed. The results showed that the heat transfer performance was better at larger mass flux and lower operating pressures. Also, numerically studies carried out with new channel shapes of PCHE, *i.e.*, a zigzag with an inserted straight channel and a zigzag channel with radian, for the pressure drop and heat transfer performances of supercritical LNG [29]. The results showed that the zigzag with a 4 mm inserted straight channel had the best performance due to a higher performance evaluation criteria value at lower mass flow rates. Besides, Zhang *et al.* [30] investigated thermal characteristics of NG with phase change from supercritical state to liquid state in a straight channel PCHE. It was found that specific heat and mass flow rate of both two fluids are revealed to have the most important impact on local thermal characteristics. Yoon *et al.* [31] performed a structural simulation to find the optimal design of channels for developing PCHE on floating storage and regasification units. The results indicated that the deformation caused from the diffusion bonding process at high temperature was predicted through analysis. This method can be used to perform the sizing of PCHE under actual conditions.

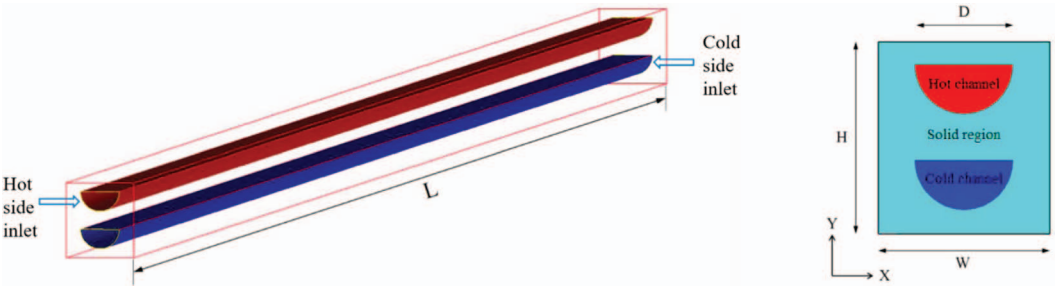

Fig. 1. Computational model of straight channels.

Recent studies have focused on thermal-hydraulic performances of a PCHE using supercritical LNG, since PCHE is deeming as the most promising candidate for cryogenic heat transfer process. However, there is still a lack of systematic correlations for Nu and f of supercritical LNG flow in a PCHE channel. So, using supercritical methane–ethane mixture as LNG, this paper numerically simulated flow and heat transfer of supercritical methane–ethane mixture in a straight PCHE channel, considering the influence of operating pressure, inlet temperature and mass flux. Meanwhile, based on numerical results, the correlations for Nu and f of supercritical methane–ethane mixture flow were proposed, which could be used for the design of PCHE in LNG-FPSO.

2 Numerical schemes

2.1 Computational model and boundary conditions

In this study, considering the periodic characteristics of channels in PCHE, only one couple of hot and cold channels, as well as the corresponding solid plate, are used for simulations, as shown in Figure 1. In fact, by setting periodic boundary conditions, a set of hot and cold channels can reflect the thermal-hydraulic characteristics of the whole heat-exchange part in PCHE. de la Torre *et al.* [32] compare the temperature distribution along the channel between one, three, five, and seven couple of hot and cold channels. The deviation between the one couple channels and the seven couple ones was 3.34% in their study, which was acceptable. Considering the computational speed, almost all numerical studies on PCHE took a couple of hot and cold channels as the research object [6, 33, 34]. The simulation is on cross flow in the PCHE channel with a full length (L) of 200 mm, the height (H) of 2.92 mm and the width of 2.62 mm, using supercritical methane–ethane mixture in hot side and water in cold side. The straight channels have a diameter of 1.51 mm and SS316L stainless steel is chosen as solid material with a thermal conductive coefficient of 14.6 W/(m K).

In simulations, the top and bottom surfaces are defined as periodic boundary conditions, and other surfaces are defined as adiabatic boundary conditions. In cold channel, the mass flow rate is 5×10^{-4} kg/s, the inlet temperature is 296 K and the outlet pressure is 0.6 Mpa. In all cases, parameters in the cold channel are kept constant. For hot channels, the inlet and outlet conditions are changed for different simulation cases.

2.2 Thermo-physical properties of supercritical methane

In this paper, methane–ethane mixture (the mole ratio 9:1) is used to substitute NG. The pressure and temperature of methane–ethane mixture range from 6.5 MPa to 9.5 MPa and from 373 K to 423 K, respectively, which have exceeded the critical pressure and temperature (P_{cr} = 5.822 MPa, T_{cr} = 209.96 K). So, the methane–ethane mixture flow is in a supercritical state. Thermo-physical properties of supercritical methane–ethane mixture, including specific heat capacity at constant pressure, density, thermal conductivity and dynamic viscosity, are calculated from NIST database, as shown in Figure 2. It is clear that thermo-physical properties of supercritical fluid dramatically change obviously during the selected temperature range. Accordingly, these thermo-physical properties are fitted with polynomial functions of temperature in the range of 290–460 K, as shown in Table 1. The correlation coefficient R^2 is closed to 1.0 and the errors between fitting results and actual physical parameters are all in 1%. It indicates that polynomials can correctly reflect physical properties of supercritical methane–ethane mixture.

2.3 Calculation method and grid independent

The commercial software *ANSYS Fluent* is employed for simulation in this paper. In the simulation, the flow through the channel is in turbulent state and the SST $k-\omega$ turbulence model is chosen for its prominent prediction of thermal performance in supercritical flows [25, 27–30]. A detailed description of the SST $k-\omega$ turbulent model can be found in Ref. [28]. SIMPLE algorithm is applied to resolve the coupling of pressure and velocity. The residual for each variable is required to be less than 10^{-6}. The second-order upwind is used to discretize convection and diffusion terms in the moment equation and energy equation so as to ensure the accuracy of simulations.

The model and flow parameters of Meshram *et al.* [14] are chosen as the baseline model. The mesh dependence test dominates the number of grids that going to use in the simulation. As shown in Figure 3, the influence of mesh on the accuracy of numerical results is investigated by comparing five sets of grid numbers. By comparing temperature drop and pressure drop in the straight channel, the optimal mesh of 1 052 000 grid numbers was selected in consideration of the accuracy and computational efficiency. For this case, eight boundary layers were established in cross section of

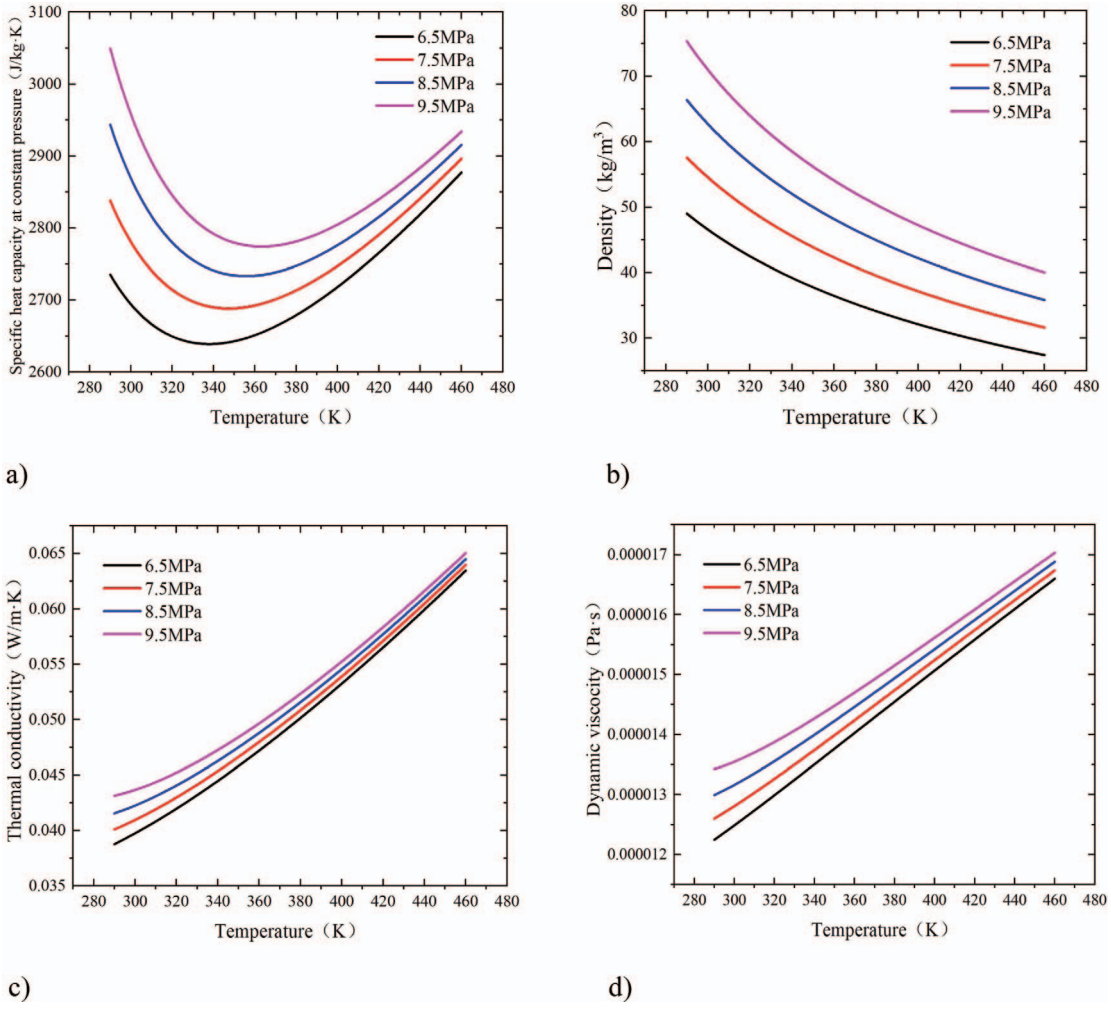

Fig. 2. Thermo-physical properties of supercritical methane–ethane mixture under different pressures. (a) Specific heat capacity, (b) density, (c) thermal conductivity, (d) dynamic viscosity.

Table 1. Polynomial functions of thermal-physical properties of supercritical methane–ethane mixture.

Pressure	Fitting polynomials	R^2
6.5 MPa	$\rho = 410.41503 - 2.50197\,T + 0.00572\,T^2 - 4.52612\mathrm{e}^{-6}\,T^3$	0.984
	$C_p = 46644.93859 - 445.08496\,T + 1.68068\,T^2 - 0.00282\,T^3 + 1.77737\mathrm{e}^{-6}\,T^4$	0.987
	$\lambda = 0.09526 - 5.77614\mathrm{e}^{-4}\,T + 1.66724\mathrm{e}^{-6}\,T^2 - 1.24604\mathrm{e}^{-9}\,T^3$	0.976
	$\mu = 1.52342\mathrm{e}^{-5} - 5.63662\mathrm{e}^{-8}\,T + 2.12546\mathrm{e}^{-10}\,T^2 - 1.82111\mathrm{e}^{-13}\,T^3$	0.989
	$\rho = 568.10754 - 3.6265\,T + 0.00854\,T^2 - 6.917\mathrm{e}^{-6}\,T^3$	0.975
7.5 MPa	$C_p = 69191.16168 - 683.63252\,T + 2.63117\,T^2 - 0.0045\,T^3 + 2.89452\mathrm{e}^{-6}\,T^4$	0.993
	$\lambda = 0.13861 - 9.04275\mathrm{e}^{-4}\,T + 2.50632\mathrm{e}^{-6}\,T^2 - 1.96848\mathrm{e}^{-9}\,T^3$	0.986
	$\mu = 2.50538\mathrm{e}^{-5} - 1.282\mathrm{e}^{-7}\,T + 3.93625\mathrm{e}^{-10}\,T^2 - 3.35878\mathrm{e}^{-13}\,T^3$	0.987
	$\rho = 879.61022 - 5.75571\,T + 0.01363\,T^2 - 1.10187\mathrm{e}^{-6}\,T^3$	0.994
9.5 MPa	$C_p = 102257.9485 - 1014.37067\,T + 3.87505\,T^2 - 0.00658\,T^3 + 4.1888\mathrm{e}^{-6}\,T^4$	0.988
	$\lambda = 0.22995 - 1.57\mathrm{e}^{-3}\,T + 4.13639\mathrm{e}^{-6}\,T^2 - 3.31022\mathrm{e}^{-9}\,T^3$	0.985
	$\mu = 4.97667\mathrm{e}^{-5} - 3.05223\mathrm{e}^{-7}\,T + 8.26975\mathrm{e}^{-10}\,T^2 - 6.91722\mathrm{e}^{-13}\,T^3$	0.976

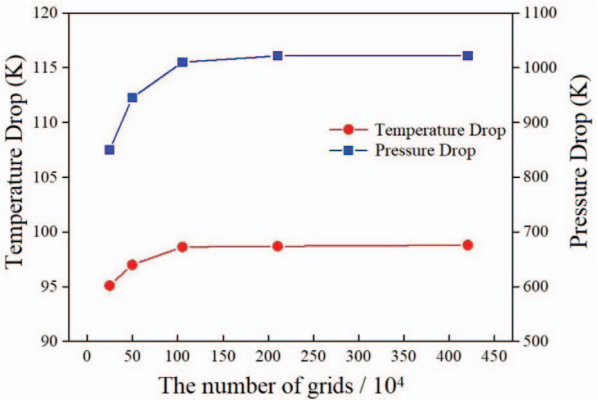

Fig. 3. Results for grid independence.

the semi-circular channel because of the strict requirement for boundary-layer grid in supercritical flow and heat transfer. The thickness of the first boundary layer was 0.001 mm and the growth factor is 1.2.

2.4 Calculation methodology

In this paper, heat transfer coefficient and pressure drop in the straight channel flow are used to analyze thermo-hydraulic characteristics of PCHE. The values of these two parameters can be obtained directly or indirectly through numerical results.

The average heat transfer coefficient can be obtained by the following equation:

$$h = \frac{q}{T_w - T_b} = \frac{q}{T_w - (T_{\text{out}} + T_{\text{in}})/2}, \tag{1}$$

where q is heat flux, T_w is the area-average wall temperature, and T_{in} and T_{out} are the inlet and outlet temperature of channel.

The Reynolds number is defined as:

$$\text{Re} = \frac{\rho_b v_b D_h}{\mu_b}, \tag{2}$$

where ρ_b, v_b and μ_b are the bulk density, velocity and dynamical viscosity, respectively; D_h is the hydraulic diameter and can be calculated as:

$$D_h = \frac{4A}{P}, \tag{3}$$

where A and P are the cross-sectional area and wetted perimeter of the semi-circular fluid channel.

Nusselt number is calculated as:

$$\text{Nu} = \frac{hD_h}{\lambda_b}, \tag{4}$$

where λ_b is the average thermal conductivity of supercritical fluid.

Fanning friction factor is expressed as:

$$f = \frac{\Delta P D_h}{2L\rho_b v_b^2}, \tag{5}$$

where ΔP and L are the frictional pressure drop and the length of semi-circular fluid channel.

2.5 Model validation

To validate the reliability of numerical results, numerical method verification is conducted. Few experiments and simulations with natural gas as working fluid in PCHE have been found. Therefore, numerical results about S–CO_2 flow in PCHE that obtained by Meshram *et al.* [14] are selected to validate the accuracy of numerical simulation in this work. The physical properties of flow media, S–CO_2, were obtained by NIST. The geometry of the PCHE channel, other boundary conditions, and numerical methods have been described in the above sections. In the validating process, the differences in temperature drop and pressure drop of cold and hot microchannels are calculated. The comparison details are shown in Table 2. The temperature ranges corresponding to the low-temperature region and high-temperature region are 400–630 K and 500–730 K, respectively. The maximum deviation of temperature drop and pressure drop between the calculated results and ones from Ref. [14] are 8.77% and −7.52%, respectively. Therefore, the numerical model and method used herein are reliable.

3 Results and discussion

3.1 Effect of operating parameters

3.1.1 Effect of inlet temperature and operating pressure

Considering complex operating conditions in practical engineering applications, in this work, the effect of inlet temperature and operating pressure on flow and heat transfer characteristics of supercritical methane–ethane mixture is mainly discussed. The operating parameters are set as: the inlet mass flow rate 600 kg/(m^2 s), three outlet pressures 6.5 MPa, 7.5 MPa and 9.5 MPa, the inlet temperature of hot channel 373–400 K. The important results are shown in Figures 4–7 at different cases (different inlet temperature and operating pressures).

Figure 4 presents the variation of heat transfer coefficient with the inlet temperature at different pressures. It can be clearly seen that: heat transfer coefficient increases almost linearly with inlet temperature, due to the smaller density and stronger turbulent intensity at a higher inlet temperature. Meanwhile, specific heat capacity at constant pressure increases with the increase of temperature during 373–400 K, which leads to much more heat transfer performance. For the effect of pressure, heat transfer coefficient also increases with operating pressure because of the increasing specific heat capacity and thermal conductivity of supercritical methane–ethane mixture at higher pressure.

Considering different flow media, the comparison of heat transfer coefficients of two supercritical flows at 6.5 MPa is carried out, as shown in Figure 5. It is found that heat transfer coefficient of supercritical methane flow is 7.01% larger in average than that of supercritical

Table 2. Comparison of the calculated results and ones from Ref. [14].

	Temperature drop in Ref. [14] (K)	Temperature drop in this study (K)	Deviation (%)	Pressure drop in Ref. [14] (Pa)	Pressure drop in this study (Pa)	Deviation (%)
Low-temperature region						
Cold channel	98.8	98.29	−0.52	1022.73	1030	−0.71
Hot channel	137.1	128.7	6.12	2755.7	2632	4.49
High-temperature region						
Cold channel	114	104	8.77	1437	1496	−4.11
Hot channel	128	120.1	6.17	3657	3932	−7.52

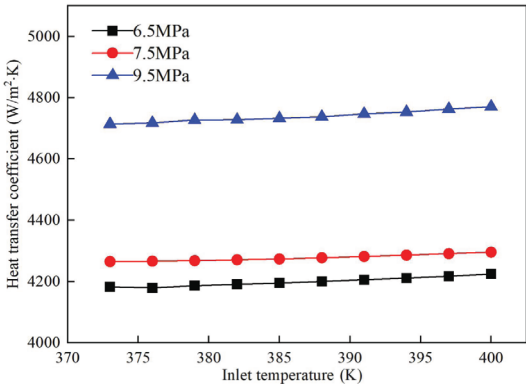

Fig. 4. The variation of heat transfer coefficient with the inlet temperature at different outlet pressures.

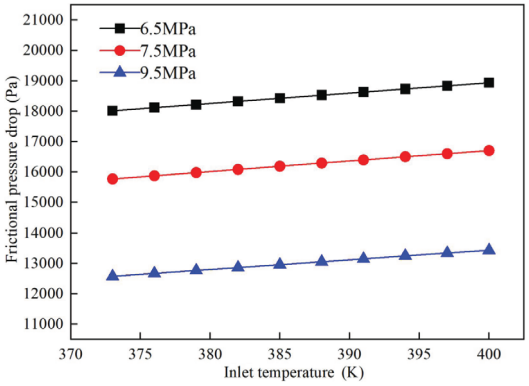

Fig. 6. The variation of frictional pressure drop with inlet temperature at different outlet pressures.

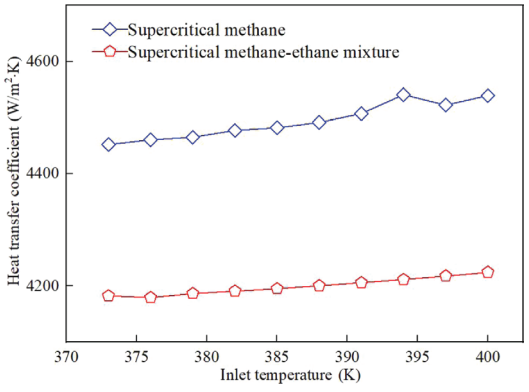

Fig. 5. Comparison of heat transfer coefficients of two supercritical flows at 6.5 MPa.

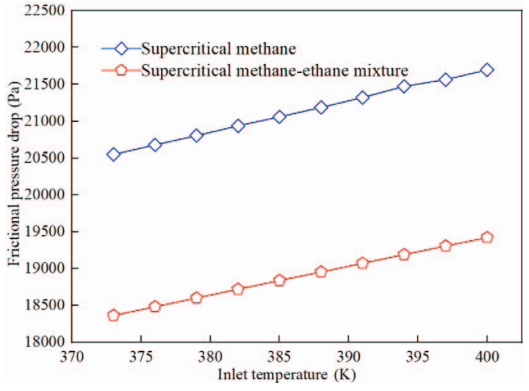

Fig. 7. Comparison of frictional pressure drops of two supercritical flows at 6.5 MPa.

methane–ethane mixture flow. The reason is that: density of supercritical methane is smaller than that of supercritical methane–ethane mixture, as shown in Figure 8a, inducing a larger velocity and more intense disturbance at a given inlet mass flux. Besides, supercritical methane has larger specific heat capacity at constant pressure, as shown in Figure 8b, which also leading to the same results above.

Figure 6 presents the variation of frictional pressure drop with the inlet temperature at different pressures. It can be seen that: frictional pressure drop is almost proportional to inlet temperature and inversely proportional to operating pressure. This may be attributed to the decreasing density with the increasing inlet temperature because smaller density results in larger velocity and causes the increase of acceleration pressure drop and frictional pressure drop. In addition, the difference of frictional pressure drop between adjacent pressures increases with the increasing operating pressure. Because the frictional pressure drop is proportional with the square of velocity, which is dominated by density and related to operating pressure.

The comparison of frictional pressure drops of two supercritical flows at 6.5 MPa is also carried out, as shown in Figure 7. Frictional pressure drop of supercritical

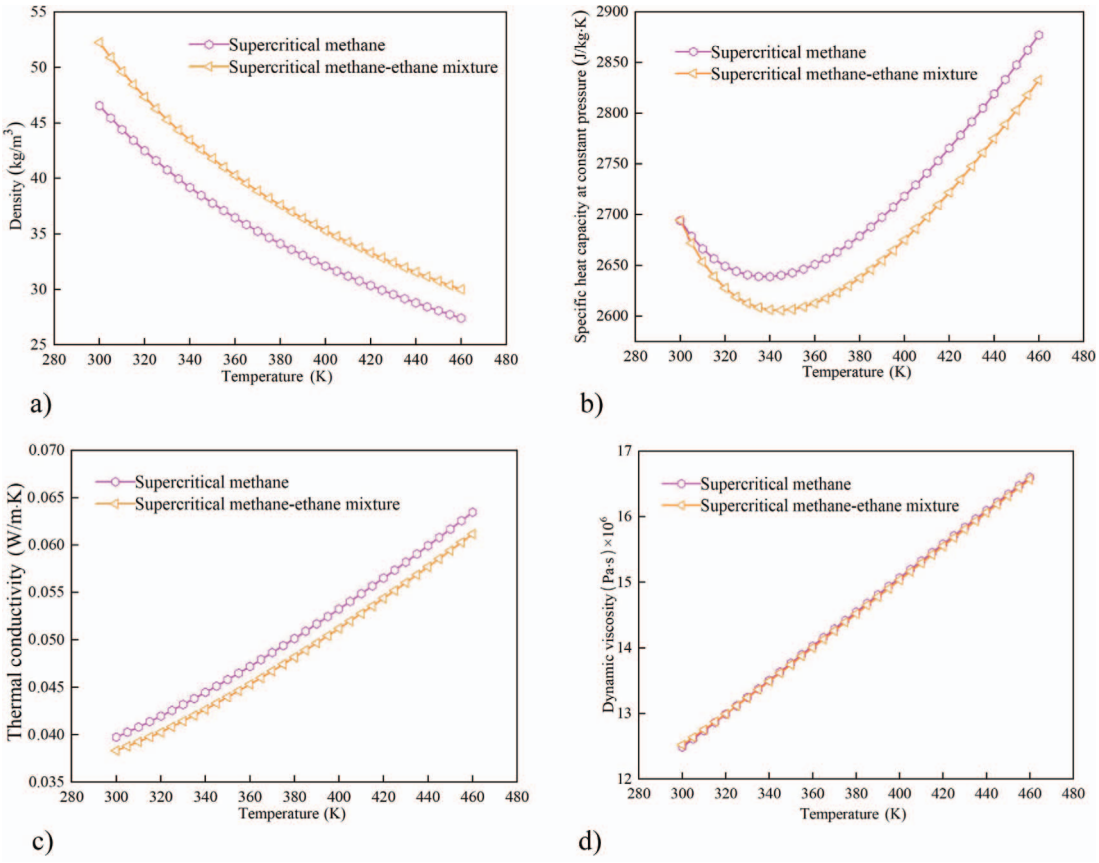

Fig. 8. Comparisons of physical parameters of supercritical methane and supercritical methane–ethane mixture at 6.5 MPa. (a) Density, (b) specific heat capacity, (c) thermal conductivity, (d) dynamic viscosity.

methane flow is much larger by 11.82% in average than that of supercritical methane–ethane mixture flow. The reason is the smaller flow velocity of supercritical methane–ethane mixture due to its larger density, as shown in Figure 8a.

3.1.2 Effect of mass flux

In this section, the effect of mass flux on thermal performance of supercritical methane–ethane mixture flow is discussed. The variation of heat transfer coefficient with Reynolds number at 383 K is shown in Figure 9. It is comprehensible that heat transfer coefficient increases with the increasing Reynolds number. While the increase of heat transfer coefficient with pressure is still caused by the increasing specific heat capacity and thermal conductivity of supercritical methane–ethane mixture at higher pressure. Also, considering different flow media, the comparison of heat transfer coefficients of two supercritical flows at 6.5 MPa is carried out in Figure 10. It is found that heat transfer coefficients of the two supercritical medias both increase with Reynolds number and in supercritical methane flow, it has a 6.93% larger value in average than that of supercritical methane–ethane mixture flow at the same Reynolds number. The reason is the same as that been discussed for Figure 5 in Section 3.1.1.

Figure 11 shows the variation of frictional pressure drop with Reynolds number at different pressures. The effect of Reynolds number on frictional pressure drop is similar to that of inlet temperature. The comparison of frictional pressure drops of two supercritical flows at 6.5 MPa is also carried out in Figure 12. It is indicated that frictional pressure drop of supercritical methane flow is 12.50% larger in average than that of supercritical methane–ethane mixture flow.

3.2 Correlations for flow and heat transfer

The correlations for flow and heat transfer parameters are very important for the design of heat exchangers. Now, correlations are mainly concentrated on straight or zigzag channels with supercritical CO_2, supercritical helium, supercritical nitrogen and water, as shown in Table 3. But, there are no correlations for supercritical methane–ethane mixture flow in PCHE channels. In some design work of PCHE for NG, correlations for other fluid media, such as CO_2, are used to calculate the heat transfer and pressure drop of NG flow in PCHE channel, which will bring significant error. So, it is necessary to evaluate the errors between existing correlations and numerical results in this work, for the proposing of new correlations for straight channel with supercritical methane at different Reynolds numbers. Through the detail analysis, correlations proposed by Zhao *et al.* [25] and Meshram *et al.* [14] are chosen for comparison with numerical results.

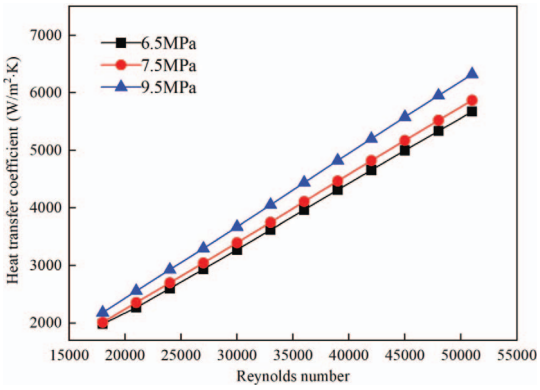

Fig. 9. The variation of heat transfer coefficient Reynolds number at different outlet pressures.

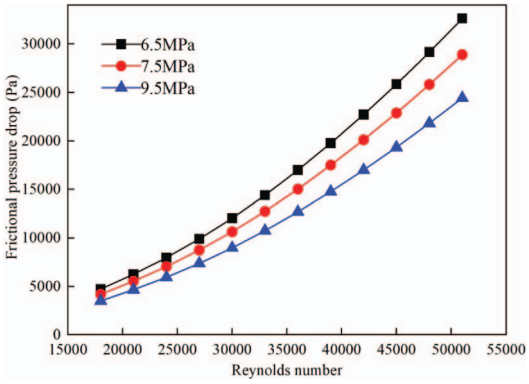

Fig. 11. The variation of frictional pressure drop with Reynolds number at different outlet pressures.

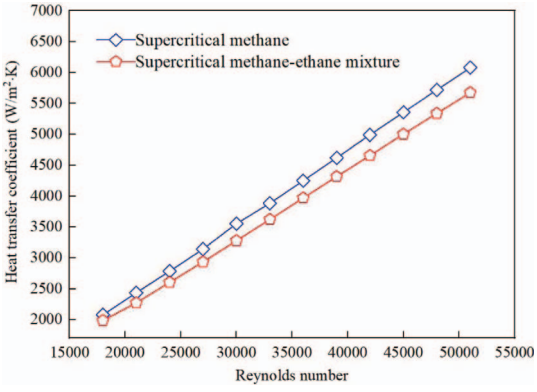

Fig. 10. Comparison of heat transfer coefficients of two supercritical flows at 6.5 MPa.

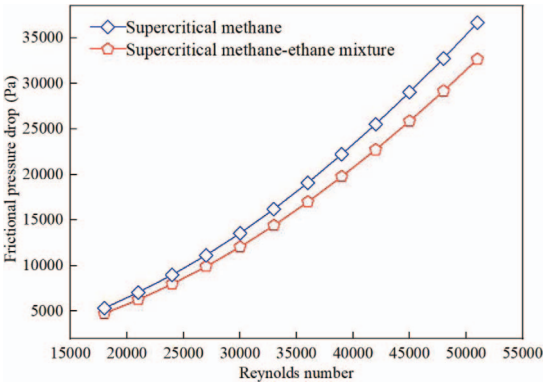

Fig. 12. Comparison of frictional pressure drops of two supercritical flows at 6.5 MPa.

Based on numerical results, the average errors of Nusselt number and Fanning fraction factor are shown in Table 4, in comparing with the values calculated by Zhao's and Meshram's correlations [14, 25]. It can be clearly seen that: it is difficult to predict flow and heat transfer characteristics of supercritical methane–ethane mixture in a straight and semi-circle channel based on existing correlations for other fluid media. Therefore, it is necessary to develop new correlations for predicting flow and heat transfer characteristics of supercritical methane–ethane mixture in a PCHE channel.

Nusselt number and Fanning friction factor of supercritical methane and supercritical methane–ethane mixture flows at 6.5 MPa are shown in Figures 13 and 14. As can be clearly seen, Nusselt number and Fanning friction factor of supercritical methane flow are both larger than that of supercritical methane–ethane mixture flow because supercritical methane has larger thermal conductivity and smaller density, as shown in Figure 8. So, neither correlations for supercritical carbon dioxide nor correlations for supercritical methane are appropriate for supercritical methane–ethane mixture flow. Therefore, new correlations need to be obtained.

Nusselt number and Fanning friction factor under different Reynolds numbers are obtained, as shown in Figures 15 and 16. Numerical results shown in Figure 15 are correlated in terms of Reynolds number and Prandtl number by using the least square method. The correlation for Nusselt number is obtained as follows:

$$\mathrm{Nu} = 0.0029\mathrm{Re}^{1.003}\mathrm{Pr}^{1.192} \quad (18\,000 < \mathrm{Re} < 51\,000). \quad (6)$$

The same method is used when fitting the correlation for Fanning friction factor, as shown as:

$$f = -0.107\mathrm{Re}^{0.00746} + 0.121 \quad (18\,000 < \mathrm{Re} < 51\,000). \quad (7)$$

In order to validate the accuracy of new correlations, several cases under different Reynolds numbers at 8.5 MPa were calculated. The results calculated from correlations of Nusselt number and Fanning friction factor are compared with numerical results, as shown in Figures 17 and 18. It is found that the maximum error of Nusselt number is less than 1.0%, and the maximum error of Fanning friction factor is −1.22%, when comparing calculated results with simulation results. Therefore, new correlations for supercritical methane–ethane mixture flow have reliable accuracy.

Table 3. Correlations for Nusselt number and Fanning fraction factor in PCHE channels with different fluids.

References	Channel shape	Working fluid	Correlations for Nusselt number	Application conditions
Kim *et al.* [35]	Straight	Water	$0.7203\ \mathrm{Re}^{0.1775}\ \mathrm{Pr}^{1/3}\left(\frac{\mu_b}{\mu_w}\right)^{0.14}$ $1.3383\ \mathrm{Re}^{-0.5003}$	$100 < \mathrm{Re} < 850$
Zhao *et al.* [25]	Straight	Nitrogen	$0.3791\ \mathrm{Re}^{0.5887}\ \mathrm{Pr}^{0.288}$ $33.24\ \mathrm{Re}^{-0.8304} + 0.0002596$	$19379 < \mathrm{Re} < 40\ 171$
Meshram *et al.* [14]	Straight	CO_2	$0.0718\ \mathrm{Re}^{0.71}\ \mathrm{Pr}^{0.55}$ $0.8657\ \mathrm{Re}^{-0.5755} + 0.00405$	$5000 < \mathrm{Re} < 26\ 000$
Kwon *et al.* [36]	Zigzag	Water	$0.278\ \mathrm{Re}^{0.452}\left(\frac{h}{p}\right)^{0.051}\mathrm{Pr}^{0.333}$ $95.431\left(\frac{1}{\mathrm{Re}}\right)^{0.863}\left(\frac{h}{p}\right)^{0.396}\mathrm{Pr}^{0.333}$	$150 < \mathrm{Re} < 800$
Kim and No [37]	Zigzag	Helium	$4.089 + 0.00365\ \mathrm{Re}^{1.0}\ \mathrm{Pr}^{0.58}$ $\frac{15.78}{\mathrm{Re}} + 0.0487\ \mathrm{Re}^{-0.16}$	$0 < \mathrm{Re} < 2500$, $0.66 < \mathrm{Pr} < 13.41$
Chen *et al.* [38]	Zigzag	Helium	$0.005516 \pm 0.0016\ \mathrm{Re}^{0.69195 \pm 0.00559}$ $17.639\ \mathrm{Re}^{0.8861 \pm 0.0017}$	$1400 < \mathrm{Re} < 2200$
Nikitin *et al.* [18]	Zigzag	CO_2	Hot channel: $h = 2.52\ \mathrm{Re}^{0.681}\ (-1.402\mathrm{e}^{-6} \pm 0.087\mathrm{e}^{-6})$ $\mathrm{Re} + (0.04495 \pm 0.00038)$	Hot channel: $2800 < \mathrm{Re} < 5800$
			Cold channel: $h = 5.49\ \mathrm{Re}^{0.625}\ (-1.545\mathrm{e}^{-6} \pm 0.099\mathrm{e}^{-6})$ $\mathrm{Re} + (0.09318 \pm 0.0009)$	Cold channel: $6200 < \mathrm{Re} < 12\ 100$
Baik *et al.* [20]	Zigzag	CO_2	$0.8405\ \mathrm{Re}^{0.5704}\ \mathrm{Pr}^{1.08}$ $0.0748\ \mathrm{Re}^{-0.19}$	$15\ 000 < \mathrm{Re} < 85\ 000$

Table 4. The average errors of Nu and f compared with ones predicted by Zhao's and Meshram's correlations.

Pressure (MPa) Average error (%)		6.5	7.5	9.5
Nu	Zhao *et al.* [25]	90.95	88.59	81.41
	Meshram *et al.* [14]	21.33	19.43	14.56
f	Zhao *et al.* [25]	10.46	40.38	10.67
	Meshram *et al.* [14]	16.79	17.23	17.73

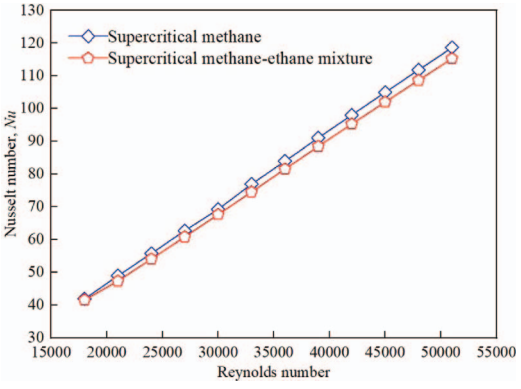

Fig. 13. The variation of Nusselt number with Reynolds number at 6.5 MPa.

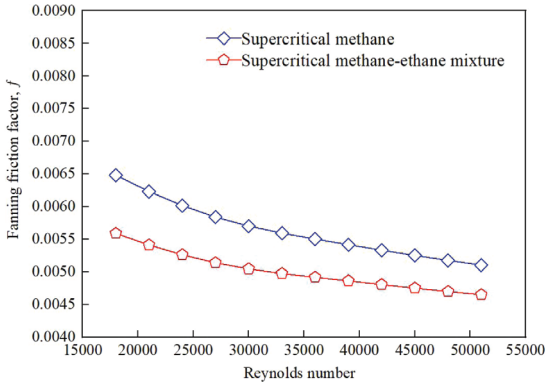

Fig. 14. The variation of Fanning friction factor with Reynolds number at 6.5 MPa.

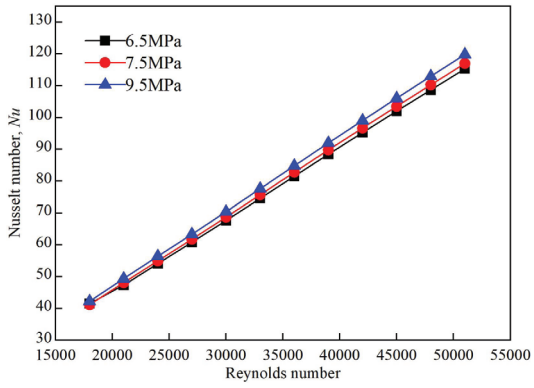

Fig. 15. The variation of Nusselt number with Reynolds number at different outlet pressures.

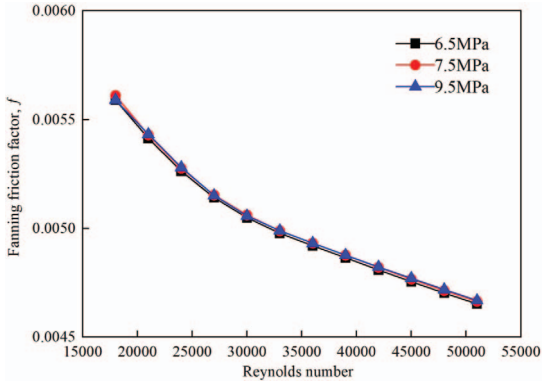

Fig. 16. The variation of Fanning friction factor with Reynolds number at different outlet pressures.

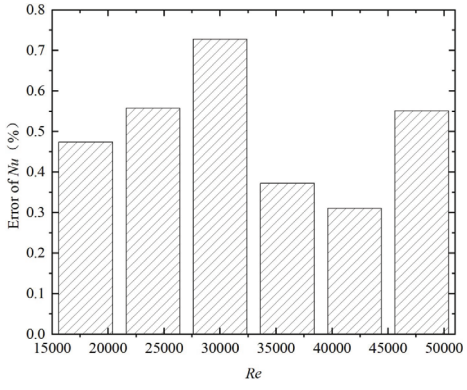

Fig. 17. Comparison of Nusselt number between calculated results and numerical results.

4 Conclusion

In this paper, the thermal-hydraulic performance of supercritical methane–ethane mixture flow in a PCHE straight channel is investigated. Some important conclusions are drawn as follows:

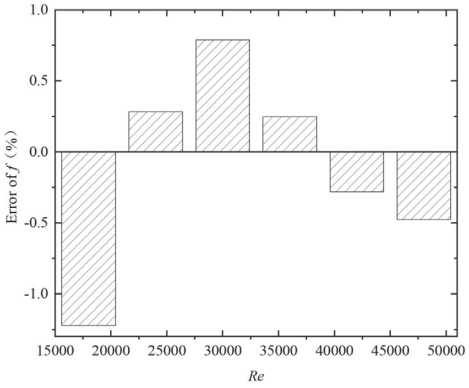

Fig. 18. Comparison of Fanning friction factor between calculated results and numerical results.

1. The effects of operating parameters on heat transfer coefficient and frictional pressure drop of supercritical methane–ethane mixture flow are similar to those of supercritical methane flow. Higher pressure, inlet temperature and mass flux are beneficial to heat transfer.
2. Heat transfer coefficient and frictional pressure drop of supercritical methane–ethane mixture flow are smaller than those of supercritical methane flow. The main reason is the difference of physical properties.
3. Through detail comparisons, it is found that the existing correlations, based on data from S–CO_2 flow *et al.*, are not suitable for supercritical methane–ethane mixture flow in a straight and semi-circle channel. Therefore, based on numerical results, new correlations within certain Reynolds number range are proposed for supercritical methane–ethane mixture flow in a PCHE straight channel.

Acknowledgments. The authors are grateful for the support of *Science and Technology Development Project of Jilin Province* (No. 20200403144SF).

References

1 Ren Y., Cai W.H., Jiang Y.Q. (2018) Numerical study on shell-side flow and heat transfer of spiral-wound heat exchanger under sloshing working conditions, *Appl. Therm. Eng.* **134**, 287–297.
2 White J., Longley H. (2009) FLNG technology shows promise for stranded gas fields, *Offshore* **69**, 11, 78.
3 Zhao W.H., Yang J.M., Hu Z.Q., Wei Y.F. (2011) Recent developments on the hydrodynamics of Floating Liquid Natural Gas (FLNG), *Ocean Eng.* **38**, 14–15, 1555–1567.
4 Blume A. (2013) FLNG needs offshore know-how, *Hydrocarbon Process.* **92**, 1, 15–18.
5 Kim I.H., No H.C. (2011) Thermal hydraulic performance analysis of a printed circuit heat exchanger using a helium-water test loop and numerical simulations, *Appl. Therm. Eng.* **31**, 4064–4073.
6 Aneesh A.M., Sharma A., Srivastava A., Vyas K.N., Chaudhuri P. (2016) Thermal-hydraulic characteristics and performance of 3D straight channel based printed circuit heat exchanger, *Appl. Therm. Eng.* **98**, 474–482.

7 Liu S.H., Huang Y.P., Wang J.F. (2018) Theoretical and numerical investigation on the fin effectiveness and the fin efficiency of printed circuit heat exchanger with straight channels, *Int. J. Therm. Sci.* **132**, 558–566.

8 Chen M.H., Sun X.D., Christensen R.N., Skavdahl I., Utgikar V., Sabharwall P. (2018) Dynamic behavior of a high-temperature printed circuit heat exchanger: Numerical modeling and experimental investigation, *Appl. Therm. Eng.* **135**, 246–256.

9 Heatric (2011) *Compact diffusion-bonded heat exchangers – The future of heat transfer engineering*, Heatric Division of Meggitt (UK) Limited, Dorset, UK.

10 Song H. (2007) *Investigations of a printed circuit heat exchanger for supercritical CO_2 and water*, State University, Kansas.

11 Chai L., Tassou S.A. (2009) Numerical study of the thermo-hydraulic performance of printed circuit heat exchangers for supercritical CO_2 Brayton cycle applications, *Energy Procedia* **161**, 480–488.

12 Jeon S., Baik Y.J., Byon C. (2016) Thermal performance of heterogeneous PCHE for supercritical CO_2 energy cycle, *Int. J. Heat Mass Trans.* **102**, 867–876.

13 Marchionni M., Chai L., Bianchi G. (2019) Numerical modelling and performance maps of a printed circuit heat exchanger for use as recuperator in supercritical CO_2 power cycles, *Energy Procedia* **161**, 472–479.

14 Meshram A., Jaiswal A.K., Khivsara S.D., Ortega J.D., Ho C., Bapat R., Dutta P. (2016) Modeling and analysis of a printed circuit heat exchanger for supercritical CO_2 power cycle applications, *Appl. Them. Sci.* **109**, 861–870.

15 Lee S.M., Kim K.Y. (2014) A parametric study of the thermal-hydraulic performance of a zigzag printed circuit heat exchanger, *Heat Transf. Eng.* **35**, 13, 1192–1200.

16 Zheng Z.Y., Fletcher D.F., Haynes B.S. (2014) Transient laminar heat transfer simulations in periodic zigzag channels, *Int. J. Heat Mass Trans.* **71**, 758–768.

17 Yang Y., Li H.Z., Yao M.Y., Gao W., Zhang Y.F., Zhang L. (2019) Investigation on the effects of narrowed channel cross-sections on the heat transfer performance of a wavy-channeled PCHE, *Int. J. Heat Mass Trans.* **135**, 33–43.

18 Nikitin K., Kato Y., Ngo L. (2006) Printed circuit heat exchanger thermal-hydraulic performance in supercritical CO_2, experimental loop, *Int. J. Refrig.* **29**, 5, 807–814.

19 Ishizuka T., Kato Y., Muto Y., Nikitin K., Lam N.T. (2006) Thermal-hydraulic characteristics of a printed circuit heat exchanger in a supercritical CO_2 loop, *Nucl. React. Therm. Hydraul.* **30**, 109–116.

20 Baik S., Kim S.G., Lee J., Lee J.I. (2017) Study on CO_2-water printed circuit heat exchanger performance operating under various CO_2 phases for S-CO_2 power cycle application, *Appl. Therm. Eng.* **113**, 1536–1546.

21 Bae S.J., Kwon J., Kim S.G., Son I.W., Lee J.I. (2019) Condensation heat transfer and multi-phase pressure drop of CO_2 near the critical point in a printed circuit heat exchanger, *Int. J. Heat Mass Trans.* **129**, 1206–1221.

22 Hu H., Li J., Chen Y., Xie Y. (2021) Measurement and correlation for two-phase frictional pressure drop characteristics of flow boiling in printed circuit heat exchangers, *Int. J. Refrig.* **129**, 69–77.

23 Hu H., Li J., Xie Y., Chen Y. (2021) Experimental investigation on heat transfer characteristics of flow boiling in zigzag channels of printed circuit heat exchangers, *Int. J. Heat Mass Trans.* **165**, 120712.

24 Kim S.G., Lee Y., Ahn Y., Lee J.I. (2016) CFD aided approach to design printed circuit heat exchangers for supercritical CO_2 Brayton cycle application, *Ann. Nucl. Energy* **92**, 175–185.

25 Zhao Z.C., Zhang X., Zhao K., Jiang P.P., Chen Y.P. (2017) Numerical investigation on heat transfer and flow characteristics of supercritical nitrogen in a straight channel of printed circuit heat exchanger, *Appl. Therm. Eng.* **126**, 717–729.

26 Kim I.H., No H.C., Lee J.I., Jeon B.G. (2009) Thermal hydraulic performance analysis of the printed circuit heat exchanger using a helium test facility and CFD simulations, *Nucl. Eng. Des.* **239**, 2399–2408.

27 Zhao Z.C., Zhao K., Jia D.D., Jiang P.P., Shen R.D. (2017) Numerical investigation on the flow and heat transfer characteristics of supercritical liquefied natural gas in an airfoil fin printed circuit heat exchanger, *Energies* **10**, 11, 1828–1845.

28 Zhao Z.C., Zhou Y.M., Ma X.L., Chen X.D., Li S.L., Yang S. (2019) Numerical study on thermal hydraulic performance of supercritical LNG in zigzag-type channel PCHEs, *Energies* **12**, 3, 548–566.

29 Zhao Z.C., Zhou Y.M., Ma X.L., Chen X.D., Li S.L., Yang S. (2019) Effect of different zigzag channel shapes of PCHEs on heat transfer performance of supercritical LNG, *Energies* **12**, 11, 2085–2099.

30 Zhang P., Ma T., Ke H.B., Wang W., Lin Y.S., Wang Q.W. (2019) Numerical investigation on local thermal characteristics of printed circuit heat exchanger for natural gas liquefication, *Energy Procedia* **158**, 5408–5413.

31 Yoon S.H., Shin J.H., Kim D.H., Choi J.S. (2017) Design of printed circuit heat exchanger (PCHE) for LNG re-gasification system, in: *Proceeding of the ASME 2017 Int. Mech. Eng. Congr. Exp.*, Tampa, Florida, USA, November 3–9, 2017.

32 de la Torre R., François J., Lin C. (2021) Optimization and heat transfer correlations development of zigzag channel printed circuit heat exchangers with helium fluids at high temperature, *Int. J. Therm. Sci.* **160**, 106645.

33 Peng Z.R., Zheng Q.Y., Chen J., Yu S.C., Zhang X.R. (2020) Numerical investigation on heat transfer and pressure drop characteristics of coupling transcritical flow and two-phase flow in a printed circuit heat exchanger, *Int. J. Heat Mass Trans.* **153**, 119557.

34 Zhou Y.L., Yin D.D., Guo X.T. (2022) Numerical analysis of the thermal and hydraulic characteristics of CO_2/propane mixtures in printed circuit heat exchangers, *Int. J. Heat Mass Trans.* **185**, 122434.

35 Kim Y.H., Seo J.E., Choi Y.J., Lee K.J. (2008) Heat transfer and pressure drop characteristics of straight channel of printed circuit heat exchangers, *Trans. Korean Soc. Mech. Eng. B* **32**, 12, 915–923.

36 Kwon O.K., Choi M.J., Choi Y.J. (2009) Heat transfer and pressure drop characteristics in zigzag channel angles of printed circuit heat exchangers, *Korean J. Air-Cond. Refrig. Eng.* **21**, 9, 475–482.

37 Kim I.H., No H.C. (2013) Thermal-hydraulic physical models for a printed circuit heat exchanger covering He, He-CO_2 mixture, and water fluids using experimental data and CFD, *Exp. Therm. Fluid Sci.* **48**, 213–221.

38 Chen M.H., Sun X.D., Christensen R.N., Skavdahl I., Utgikar V., Sabharwall P. (2016) Pressure drop and heat transfer characteristics of a high-temperature printed circuit heat exchanger, *Appl. Therm. Eng.* **108**, 1409–1417.